

Polarization-dependence of palladium deposition on ferroelectric lithium niobate (0001) surfaces

Seungchul Kim, Michael Rutenberg Schoenberg, and Andrew M. Rappe*

*The Makineni Theoretical Laboratories, Department of Chemistry,
University of Pennsylvania, Philadelphia, Pennsylvania 19104-6323, USA*

(Dated: July 14, 2021)

We investigate the effect of ferroelectric polarization direction on the geometric properties of Pd deposited on the positive and negative surfaces of LiNbO₃ (0001). We predict preferred geometries and diffusion properties of small Pd clusters using density functional theory, and use these calculations as the basis for kinetic Monte Carlo simulations of Pd deposition on a larger scale. Our results show that on the positive surface, Pd atoms favor a clustered configuration, while on the negative surface, Pd atoms are adsorbed in a more dispersed pattern due to suppression of diffusion and agglomeration. This suggests that the effect of LiNbO₃ polarization direction on the catalytic activity of Pd [J. Phys. Chem. **88**, 1148 (1984)] is due, at least in part, to differences in adsorption geometry. Further investigations using these methods can aid the search for catalysts whose activities switch reversibly with the polarization of their ferroelectric substrates.

PACS numbers: 68.43.Jk,68.43.Bc,82.65.+r,77.84.Ek

The spontaneous polarization of ferroelectric materials has enabled their use in technological devices ranging from SONAR to random access memory. While most current applications of ferroelectrics result primarily from their bulk properties, polarization can also impact the surface properties of these materials, including surface stoichiometry [1–3], geometry [2, 3], and electronic structure [1, 3–5]. These polarization dependent differences in intrinsic surface properties also affect their interactions with adsorbates, [6–13] as evidenced by differences in adsorption energies [6–10] or the rates of surface catalyzed reactions [11–13]. Polarization orientation can, in turn, affect the chemical properties of the adsorbates themselves. For example, Inoue *et al.* [11] showed that the activation barrier for CO oxidation by Pd adsorbed on a LiNbO₃ surface changes by 30 kJ/mol, depending on polarization orientation. The notion that a ferroelectric substrate’s polarization can affect the activity of a supported catalyst suggests the intriguing possibility that the activity of a catalyst could be modulated reversibly by switching the polarization of a ferroelectric substrate.

Despite ample evidence showing that metals on oppositely poled ferroelectric surfaces have different catalytic properties, the mechanism underlying these differences is not well understood. The most prevalent explanation for this phenomenon has been that the difference in charge between the two surfaces alters the electronic properties of the catalyst [4, 11–13]. However, this explanation may be incomplete, as metal adsorption geometries significantly impact their catalytic properties [14]. Since ferroelectric surfaces may have different geometries depending on the sign of their polarization [1–3], it is plausible that the geometries of metals adsorbed onto them also differ [10, 15]. Two recent studies of Pd adsorption on oppositely poled LiNbO₃ (0001) surfaces present conflicting conclusions regarding the possible effect of po-

larization on metal adsorption geometry. Yun *et al.* [15] showed that large Pd clusters form on both the positive (c^+) and negative (c^-) surfaces of LiNbO₃, suggesting that polarization has little impact on metal adsorption geometry. In contrast, Zhao *et al.* [10] observed large Pd clusters only on the c^+ surface, and a more planar geometry on the c^- surface, suggesting that polarization strongly affects metal adsorption geometry. In addition, only Zhao *et al.* observed a difference in CO temperature programmed deposition between the two surfaces, suggesting that when polarization affects the activity of adsorbed catalysts, it does so, at least in part, by altering their geometries.

In view of the ambiguity of experimental investigations of the relationship between polarization and metal adsorption geometry, we address this question on a microscopic level using theoretical methods. Here we investigate the energetics and kinetics of Pd deposition on LiNbO₃ (0001) surfaces using a combination of density functional theory (DFT) calculations and kinetic Monte Carlo (KMC) simulations. We first calculate the adsorption geometries of clusters on the c^+ and c^- surfaces. We then model the range of possible diffusion and agglomeration processes of these clusters using the nudged elastic band (NEB) method [16]. Finally, we use the activation barriers of these processes as inputs for a KMC simulation of the deposition of Pd on LiNbO₃ on a larger scale. To our knowledge, this is the first theoretical study of metal adsorption kinetics on a ferroelectric surface.

In all DFT calculations, we studied five trilayer thick LiNbO₃ slabs with $\sqrt{3} \times \sqrt{3}$ surface supercells (Supplementary Fig. S1). We passivated surface charges with one Li atom per primitive supercell on the c^+ surface, and one O and one Li atom on c^- , in accordance with the findings of Levchenko and Rappe that this is the most thermodynamically stable surface composition for

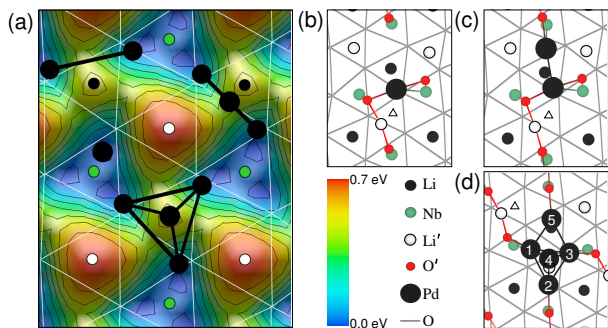


FIG. 1: (Color online) (a) Left Side: Monomeric potential energy surface and minimum energy geometries of Pd₁, Pd₂, Pd₃ and Pd₄ on c^+ . Contour spacing is 0.1 eV. Right side: Minimum energy geometries of (b) Pd₁, (c) Pd₂, and (d) Pd₅ on c^- . Triangles are original positions of Li'. The geometries for Pd₃ and Pd₄ are similar to those of atoms 1-2-3 and 1-2-3-4 in (d).

LiNbO₃ [2]. Hereafter, we denote these passivation atoms as Li' and O'. To remove spurious interactions between slabs in different supercells, we separated the slabs with more than 13 Å of vacuum and employed a dipole correction [17]. DFT total energy calculations [18] were performed using the generalized gradient approximation (GGA-PBE) [19] and implemented using the Quantum Espresso package [20]. Atoms were represented using norm-conserving nonlocal pseudopotentials [21, 22] generated using the OPIUM code [23]. We allowed relaxation of Pd atoms and the first two layers of the LiNbO₃ surface, but kept the remaining portion of the slab fixed.

Our DFT results for Pd adsorption show differences in preferred binding geometries and diffusion barriers between the c^+ and c^- surfaces. On the c^+ surface, Pd adsorption minimally changes the geometry of the LiNbO₃ surface itself. As a result, the monomeric potential energy surface (PES, Fig. 1(a)) essentially determines the geometries of multiple Pd atoms adsorbed on this surface. In particular, all Pd atoms that we predict to bind directly to the c^+ surface prefer sites close to monomeric potential energy minima. However, because the distances between minima do not match well with optimal Pd-Pd bond lengths, binding of large numbers of Pd atoms both to the c^+ surface and to each other is unfavorable. For example, adsorption geometries of three and four Pd atoms both include one atom that bonds only to other Pd atoms and does not interact directly with the surface (Fig. 1(a)). Further, we found no metastable planar structure of four atoms, suggesting that the Pd agglomeration barrier on the c^+ surface is negligible.

Diffusion and agglomeration processes on the c^+ surface are also impacted by the monomeric PES. In the monomeric case, this relationship is direct, as the two unique paths for monomer hopping (Fig. 2(a)) are the only paths containing saddle points on the PES. Be-

cause the diffusion processes of clusters of up to four atoms on the c^+ surface are dominated by the movement of a single atom, they have diffusion barriers similar to monomer hopping, a fact that can also be explained by the monomeric PES. For example, in dimer walking, a process in which one atom in a dimer steps between two potential minima and stays bonded to the other Pd, paths 2 and 3 have activation barriers similar to monomer hopping paths 1 and 2, respectively (Fig. 2(b)). Similarly, though dimer sliding involves movement of both Pd atoms, one stays adjacent to the same Nb atom and thus, its movement contributes little to the activation barrier (Fig. 2(c)). Finally, because tetramer rolling requires movement of only one Pd atom out of a monomeric potential well, it too has an activation barrier similar to that of monomer hopping. The combination of low Pd diffusion barriers and a negligible agglomeration barrier suggests that formation of large Pd clusters is favorable on the c^+ surface.

In contrast to its behavior on the c^+ surface, Pd adsorption on the c^- surface substantially alters the geometry of the surface itself. This is largely due to interactions with O' atoms, which along with Li' atoms terminate the c^- surface for charge passivation [2]. The formation of Pd-O' bonds makes adsorption onto the c^- surface much more favorable than on c^+ (Supplementary Table S1). However this also leads to complex adsorption geometries, as the O' atom is free to tilt its bond to Nb substantially in order to accommodate bonding to Pd. Despite this geometric complexity, we find that the Pd adsorption geometries on the c^- surface can be understood in the context of maximizing the number of Pd-Pd and Pd-O' bonds formed. For example, this explains why the 2D planar (not shown) and 3D configurations of clusters of four or five Pd atoms on the c^- surface, which have identical numbers of Pd-Pd/Pd-O' bonds, have binding energies within 0.1 eV of one another.

The inherent assumption in this analysis, that Pd-O' and Pd-Pd bonds have similar strengths, is justified by two facts. First, the average energies of these bonds, defined as adsorption energies divided by the number of Pd-Pd and Pd-O' bonds, in clusters of 1–5 Pd atoms are uniform (1.03 ± 0.05 eV). Second, these average bond energy values are similar to bond strengths in free clusters of 2–5 Pd atoms (1.06 ± 0.08 eV). From here on, we denote Pd-Pd and Pd-O' bonds as Pd-X.

Just as Pd-X bonds are the primary contributors to the favorable adsorption energy of Pd clusters on the c^- surface, breaking these bonds, particularly Pd-O', is the primary barrier to cluster diffusion and agglomeration. Based on the argument above that Pd-X bonds have similar energies, we would expect the activation barriers for processes that require one Pd-O' bond breaking to be approximately 1 eV. However, actual activation barriers are lower, because other atoms can move to more favorable positions in the process of transition state formation.

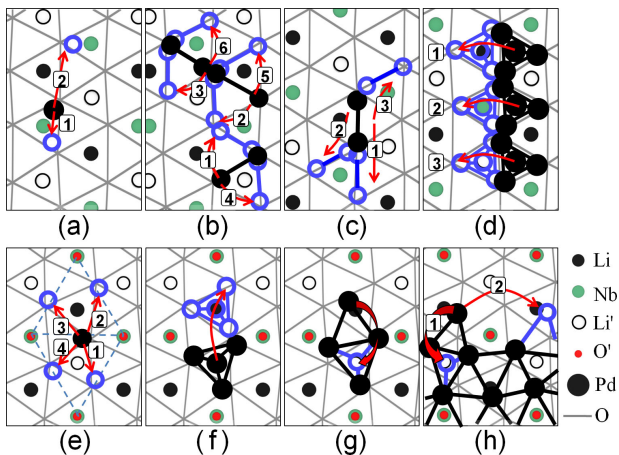


FIG. 2: (Color online) Schematic drawings of kinetic events. Top: Diffusion events on c^+ . (a) Pd₁ hopping, (b) Pd₂ walking, (c) Pd₂ sliding and (d) Pd₄ rolling. Bottom: Diffusion events on c^- . (e) Pd₁ hopping, (f) Pd₄ rolling, (g) Pd₄ agglomeration, and (h) agglomeration at large cluster (path 1) and in-plane motion (path 2). Large black circles and open blue circles denote initial and final positions for diffusion events. after the events. Blue dashed lines in (e) indicate that the monomer hops between O' bridge sites.

This is especially true when new Pd-X bonds are formed before a Pd-X bond is fully broken. Consistent with our understanding of the effect of Pd-X bond breaking on the activation barriers of diffusion processes, we find that in-plane movement at the boundary of a cluster has a high activation barrier (path 2 in Fig. 2(h)), because it requires breaking of two Pd-X bonds.

Our DFT calculations show that diffusion barriers are substantially lower on the c^+ surface ($\lesssim 0.4$ eV) than on the c^- surface ($\gtrsim 0.8$ eV). These activation energies, E_a , can be compared in a physically meaningful way when converted to expected event-event time intervals, τ , using Arrhenius kinetics [24], $\frac{1}{\tau} = \nu e^{-E_a/k_B T}$. Assuming an attempt frequency ($\nu = 10^{12}$ sec⁻¹ [25]) the time scales of diffusion events on the c^+ and c^- surfaces are on the order of microseconds and minutes, respectively. We can then infer that at a deposition rate of ≈ 0.01 – 0.1 ML/s [15], on average, each new monomer deposited on the c^+ surface will aggregate to an existing cluster before the next atom is deposited. In contrast, we would expect many Pd atoms to be deposited in the vicinity of a given Pd atom on the c^- surface between diffusion events of that atom. We thus infer that Pd atoms will agglomerate into much larger clusters on the c^+ surface than on the c^- surface of LiNbO₃.

We conducted kinetic Monte Carlo (KMC) simulations in order to characterize this inferred difference in adsorption geometries. Onto a 10 nm \times 10 nm surface, we randomly deposited Pd atoms one by one at a selected deposition rate. We then allowed Pd atoms and clusters to attempt a series of diffusion and agglomeration processes,

		path	1	2	3	4	5	6
c^+	Pd ₁ hopping		0.09	0.39				
	Pd ₂ walking		0.26	0.12	0.38	0.24	0.38	0.17
			0.32	0.02	0.41	0.24	0.38	0.17
			0.35	0.36	0.30			
	Pd ₂ sliding		0.32	0.33	0.27			
			0.23	0.19	0.27	0.24	0.11	0.18
	Pd ₃ walking		0.12	0.11	0.46	0.24	0.11	0.18
			<0.01	0.21	0.06			
	Pd ₄ rolling		0.40	0.14	0.13			
			0.55					
c^-	Pd ₁ hopping		0.82	0.87	0.87	0.82		
	Pd ₂ sliding		1.06					
	Pd ₃ flipping (Li' \rightarrow Li)		1.30	(1.31)				
	Pd ₄ rolling (Li' \rightarrow Li)		0.85	(0.70)				
	Pd ₂ dissociation		0.77					
	large cluster, in-plane		1.12					
	large cluster, agglom.		0.74	(0.93)				
Pd ₄ , agglom.		0.59	(0.61)					

TABLE I: Diffusion activation barriers (in eV) of processes drawn in Fig. 2 and described in the text. Barriers of reverse processes are written below forward processes (c^+) or in parentheses (c^-).

with probabilities based on our calculated activation barriers, at a constant attempt frequency of 10^{12} sec⁻¹ [26] for all events (Full KMC description in Supplement).

Our KMC simulations confirm that Pd forms larger clusters on the c^+ surface than on the c^- surface. Correspondingly, we find that Pd covers a much smaller area of the c^+ surface than of c^- . We also find that Pd area is insensitive to deposition rate at room temperature, as all diffusion and agglomeration processes are highly activated (for c^+) or suppressed (for c^-) at this temperature. On the c^- surface, the area covered by Pd is only affected when agglomeration plays a role, which occurs when coverage is above 0.5 ML (Fig. 3(a)). On the c^+ surface, Pd coverage area increases as temperature is lowered (Fig. 3(b)).

The relatively large diffusion barriers on the c^- surface (≈ 0.8 eV) were not sufficient to prevent agglomeration completely, especially when our simulations were extended until slightly after deposition was complete. However, we infer that the clusters on the c^- surface remain much smaller than those on the c^+ surface over a very long time scale (Supplementary Fig. S3).

Overall, our results support the conclusion of Zhao *et al.* that Pd cluster sizes are much larger on the c^+ surface than on c^- [10]. However, Yun *et al.* also produced a thorough data set supporting their conclusion that Pd forms large clusters on both surfaces of LiNbO₃ [15]. One possible explanation is that Yun and Zhao studied Pd

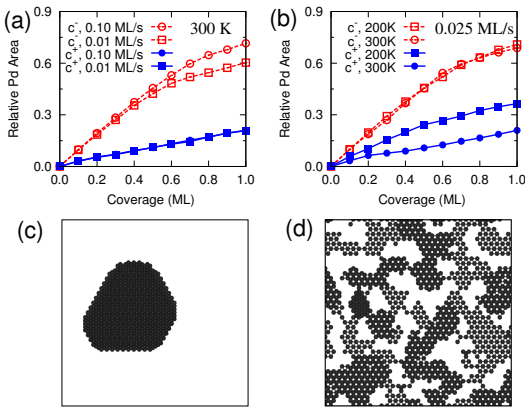


FIG. 3: (Color online) Proportion of surface area covered by Pd for simulations at a range of (a) deposition rates at 300 K and (b) temperatures with a deposition rate of 0.025 ML/s. KMC snapshots of 1.0 ML on (c) c^+ and (d) c^- at 300 K with a 0.025 ML/s deposition rate.

adsorption onto LiNbO₃ surfaces with substantially different compositions. This could be due to the presence of different impurities, such as hydroxyl groups [27], which are known to exist on some LiNbO₃ surfaces, or oxygen lattice vacancies [3]. Our calculations predict that Pd binding is weaker by 0.6 eV to a c^- surface terminated with OH instead of OLi, suggesting that agglomeration would be more favorable with some OH impurities present. Thus, it is plausible that if there were OH impurities on the c^- surface studied by Yun *et al.*, they may have influenced the formation of larger Pd clusters.

In conclusion, we find that the different surface geometries of oppositely poled LiNbO₃ (0001) surfaces lead to substantially different Pd adsorption geometries. On the c^- surface, strong Pd bonding to O', the extra surface oxygen present for charge passivation, leads to larger diffusion and agglomeration barriers. This lead in turn to less clustering and a more planar geometry overall on this surface than on c^+ . In contrast to the prevalent view that differences in catalyst charging are responsible for differences in the catalytic properties of metals adsorbed on polar ferroelectric surfaces, we conclude that the difference in adsorption geometry predicted here is sufficient to explain much of the difference in catalytic activity that has been observed for Pd deposited on oppositely poled LiNbO₃ surfaces [11]. Because formation of large Pd clusters is thermodynamically favorable on both c^+ and c^- , it is unlikely that the catalytic activity of Pd could be switched reversibly by switching the polarization of the LiNbO₃ substrate. However, the combination of theoretical methods used here is well suited for the study of other metal/ferroelectric surface combinations in search of systems with switchable catalytic activity, and the present example serves as a paradigm of polarization controlling catalytic cluster geometry and reactivity.

S. K. was supported by the US Department of Energy through grant DE-FG02-07ER15920, and A. M. R. by the Air Force Office of Scientific Research through FA9550-10-1-0248. Computational support was provided by the High-Performance Computing Modernization Office of the US Department of Defense.

* corresponding author: rappe@sas.upenn.edu

- [1] C. Noguera, *J. Phys.: Condens. Matter* **12**, R367 (2000).
- [2] S. V. Levchenko and A. M. Rappe, *Phys. Rev. Lett.* **100**, 256101 (2008).
- [3] Y. Yun, M. Li, D. Liao, L. Kampschulte, and E. I. Altman, *Surf. Sci.* **601**, 4636 (2007).
- [4] Y. Inoue, K. Sato, and S. Suzuki, *J. Phys. Chem.* **89**, 2827 (1985).
- [5] C. Park and R. T. K. Baker, *J. Phys. Chem. B* **104**, 4418 (2000).
- [6] Y. Yun and E. I. Altman, *J. Am. Chem. Soc.* **129**, 15684 (2007).
- [7] Y. Yun, L. Kampschulte, M. Li, D. Liao, and E. I. Altman, *J. Phys. Chem. C* **111**, 13951 (2007).
- [8] A. M. Kolpak, I. Grinberg, and A. M. Rappe, *Phys. Rev. Lett.* **98**, 166101 (2007).
- [9] D. Li, M. H. Zhao, J. Garra, A. Kolpak, A. Rappe, D. A. Bonnell, and J. M. Vohs, *Nature Mater.* **7**, 473 (2008).
- [10] M. S. H. Zhao, D. A. Bonnell, and J. M. Vohs, *J. Vac. Sci. Technol.* **27**, 1337 (2009).
- [11] Y. Inoue, I. Yoshioka, and K. Sato, *J. Phys. Chem.* **88**, 1148 (1984).
- [12] Y. Inoue, M. Matsukawa, and K. Sato, *J. Phys. Chem.* **96**, 2222 (1992).
- [13] N. Saito, Y. Yukawa, and Y. Inoue, *J. Phys. Chem. B* **106**, 10179 (2002).
- [14] J. K. Nørskov *et al.*, *Chem. Soc. Rev.* **37**, 2163 (2008).
- [15] Y. Yun, N. Pilet, U. D. Schwarz, and E. I. Altman, *Surf. Sci.* **603**, 3145 (2009).
- [16] G. Henkelman, B. P. Uberuaga, and H. Jónsson, *J. Chem. Phys.* **113**, 9901 (2000).
- [17] L. Bengtsson, *Phys. Rev. B* **59**, 12301 (1999).
- [18] J. Ihm, A. Zunger, and M. L. Cohen, *J. Phys. C* **12**, 4409 (1979).
- [19] J. P. Perdew, K. Burke, and M. Ernzerhof, *Phys. Rev. Lett.* **77**, 3865 (1996).
- [20] P. Giannozzi *et al.*, *J. Phys.:Condens. Matter* **21**, 395502 (2009).
- [21] A. M. Rappe, K. M. Rabe, E. Kaxiras, and J. D. Joannopoulos, *Phys. Rev. B Rapid Comm.* **41**, 1227 (1990).
- [22] N. J. Ramer and A. M. Rappe, *Phys. Rev. B* **59**, 12471 (1999).
- [23] <http://opium.sourceforge.net>.
- [24] H. Brune, *Surface Science Reports* **31**, 121 (1998).
- [25] L. Xu, G. Henkelman, C. T. Campbell, and H. Jónsson, *Surf. Sci.* **600**, 1351 (2006).
- [26] L. Xu, C. T. Campbell, H. Jónsson, and G. Henkelman, *Surf. Sci.* **601**, 3133 (2007).
- [27] T. Volk and M. Wöhlecke, *Lithium Niobate: Defects, Photorefraction and Ferroelectric Switching* (Springer, 2008).

Supplementary Material:

Polarization-dependence of palladium deposition on ferroelectric lithium niobate (0001) surfaces

Seungchul Kim, Michael Rutenberg Schoenberg, and Andrew M. Rappe*
*The Makineni Theoretical Laboratories, Department of Chemistry,
 University of Pennsylvania, Philadelphia, Pennsylvania 19104-6323, USA*
 (Dated: July 14, 2021)

ATOMIC MODEL OF LITHIUM NIOBATE SUBSTRATES

The ferroelectric phase of lithium niobate (LiNbO_3) has a bulk structure consisting of layers in a Li-O₃-Nb pattern [2]. Here we show LiNbO_3 with its thermodynamically preferred surface terminations, as predicted by Levchenko and Rappe (Fig. S1). Li atoms are added to the positive (c^+) surface, and both Li and O atoms are added to the negative surface (c^-) of LiNbO_3 for charge passivation. Passivation atoms are denoted Li' and O'. These surface terminations make the overall stoichiometry of five trilayer slab used in this study, from c^+ (left) to c^- (right), $\text{Li}'\text{-(Li-O}_3\text{-Nb)}_5\text{-Li}'\text{O}'$.

SUPPLEMENTARY DFT METHODS

In all density functional theory (DFT) calculations, we used $3 \times 3 \times 1$ k -point grids [3], plane wave energy cutoffs of 50 Ry [4], and force tolerances of 0.01 eV/Å. When necessary, we included spin as a degree of freedom in our calculations. We checked the convergence of our monomer and dimer adsorption energies calculated in $\sqrt{3} \times \sqrt{3}$ supercells on five layer thick slabs by using either $\sqrt{7} \times \sqrt{7}$ supercells or seven trilayer thick slabs. The resulting energies agreed within 0.1 eV/Pd.

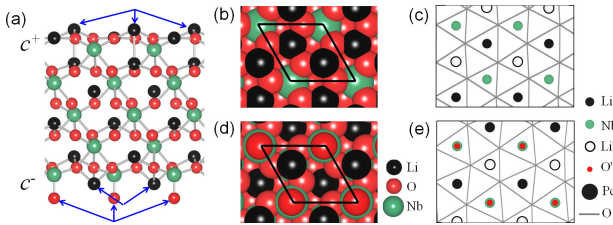


FIG. S1: Geometry of five-trilayer LiNbO_3 slab: (a) side view, (b,c) top view of c^+ , and (d,e) top view of c^- . Slabs are represented using ball and stick (a) and space filling (b,d) models, or the simplified model used in the main text (c,e). Blue arrows in (a) denote ions (Li' and O') introduced for surface charge passivation. Black lines in (b) and (d) indicate the boundaries of the LiNbO_3 primitive surface unit cell. (b) and (d) are redrawn from Ref. [1].

# of Pd atoms	positive (c^+)		negative (c^-)			free Pd_n
	E_{ads}^a	E_{ads}^c	E_{ads}^a	E_{ads}^c	$E_{bond}^{\text{Pd-X}}$	$E_{bond}^{\text{Pd-Pd}}$
1	0.95	–	2.02	–	1.01	–
2	1.20	0.62	2.01	1.44	1.01	1.15
3	1.56	0.44	2.27	1.15	1.13	1.12
4	1.84	0.26	2.34	0.77	1.02	1.05
5	–	–	2.35	0.65	0.98	0.94

TABLE S1: Per-atom adsorption energies of Pd on LiNbO_3 (LNO), relative to infinitely separated Pd atoms (E_{ads}^a) and free Pd clusters (E_{ads}^c). We define $E_{ads}^a = (E_{\text{Pd-LNO}} - E_{\text{LNO}} - nE_{\text{Pd}})/n$ and $E_{ads}^c = (E_{\text{Pd-LNO}} - E_{\text{LNO}} - E_{\text{Pd}_n})/n$, where n is the number of Pd atoms. On the c^- surface, we report average Pd-X bond energies, $E_{bond}^{\text{Pd-X}} = nE_{ads}^c/N_{bond}$, where N_{bond} is the number of Pd-X bonds. We also report average Pd-Pd bond energies, $E_{bond}^{\text{Pd-Pd}}$, in free Pd clusters for comparison. All energies are given in eV.

ADSORPTION ENERGIES

In our analysis of the energetics of Pd adsorption on LiNbO_3 , we consider two quantities for per-atom adsorption energy, E_{ads}^a and E_{ads}^c , defined as the difference between the energy of Pd-LNO and the sum of the energies of the LiNbO_3 slab and either infinitely separated (E_{ads}^a) or clustered (E_{ads}^c) Pd atoms divided by the number of Pd atoms (Table S1). We note that on the c^+ surface, E_{ads}^c becomes very small as the number of adsorbed Pd atoms increases, because of a mismatch between ideal Pd-Pd bond lengths and distances between Pd binding sites, and because most of the cluster not in contact with LNO. In contrast, E_{ads}^c remains relatively high even for pentamers on c^- , largely due to Pd-O' bonding. In the main text, we explained many of our conclusions about energetics on the c^- surface in terms of the total number of Pd-Pd and Pd-O' bonds (hereafter denoted Pd-X bonds). This analysis was justified by the fact that average Pd-X bond energies ($E_{bond}^{\text{Pd-X}}$), defined as nE_{ads}^c divided by the number of Pd-X bonds (N_{bond}), were similar for all cluster sizes studied and were also similar to average bond energies in free Pd clusters (E_{bond}^c). We show explicit values for $E_{bond}^{\text{Pd-Pd}}$ and $E_{bond}^{\text{Pd-X}}$ in Table S1.

Since Pd-O' bonding makes the key contribution to the difference in adsorption behavior between the c^+ and c^- surfaces, we wanted to be sure that DFT-GGA does not

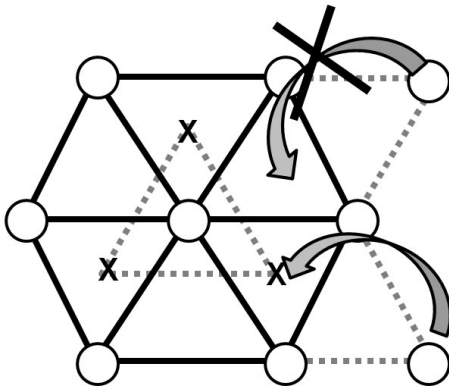


FIG. S2: An FCC lattice is not sufficient to allow all possible agglomeration events to occur. Of the two agglomeration processes pictured, one is allowed by the FCC lattice, while the other, denoted by a red 'X', would also require HCP lattice points on the second layer of the simulation lattice. We thus used an A-(ABC)-(ABC) \cdots lattice as described in the text. Open circles denote Pd atoms and 'X's denote points on the second layer of the simulation lattice.

misestimate the favorability of Pd-O interactions. To do this, we considered the case of bulk PdO. We compared our DFT-GGA energy of formation of PdO from individual Pd and O atoms, defined as $E_{\text{O}}^{\text{atom}} + E_{\text{Pd}}^{\text{atom}} - E_{\text{PdO}}$, to the sum of the experimental values for PdO formation energy [5], Pd bulk cohesive energy [6], and half of the O_2 bonding energy [7]. Our DFT-calculated value was only 2.1% greater than the experimental value, suggesting that DFT predicts Pd-O interactions well and that the strong Pd-O interactions seen on the c^- surface are valid. As a note, we did not use the DFT PdO formation energy as a metric for comparison, because DFT-GGA is known to predict the energy of O_2 quite poorly [7].

KINETIC MONTE CARLO SIMULATION DETAILS

Our kinetic Monte Carlo (KMC) simulations were performed in periodic $10 \text{ nm} \times 10 \text{ nm}$ cells. We included 15 layers of Pd binding sites above the surface, though no Pd atoms reached the top layer of the cell in any of our simulations. All Pd binding sites on the layer in contact with the LiNbO_3 surface were mapped onto their corresponding points on the triangular oxygen lattice. Beginning with the second layer above the surface, we used three sublattices to allow all possible Pd cluster configurations such that the lattice is substrate-A-(ABC)-(ABC) \cdots . The use of this lattice, which is much denser than the face-centered cubic (FCC) lattice of bulk Pd, was necessary to describe some diffusion events that can occur for small numbers of Pd atoms, but is forbidden by the FCC lattice. For example, half of all possible agglomeration processes are forbidden using an FCC lattice, because

lattice points are present that correspond to only half of the surface's hollow sites (Fig. S2). Additionally, hopping of Pd atoms between FCC and hexagonal close-packed (HCP) hollow sites on (111) cluster facets is forbidden by a pure FCC lattice. To compensate for the fact that some points in the lattice used in our simulation are closer together than a reasonable Pd-Pd bond distance, we imposed two rules. First, the same site cannot be occupied on adjacent layers of the lattice. Additionally, within the same layer, adjacent sites on different sublattices cannot be occupied.

We built our simulations primarily based on our DFT calculations of the activation barriers of diffusion and agglomeration of up to four atoms. On the c^+ surface, it was unnecessary to consider diffusion of larger clusters, because our deposition time interval was sufficiently long that we observed monomers to aggregate into clusters before other monomers are deposited in the same vicinity. Diffusion of large clusters on the c^- surface could also be neglected, because they require the breaking of two or more Pd-X bonds and thus have activation barriers sufficient to prevent their occurrence on the time scale that we considered. As described below, in cases where we had not calculated activation barriers directly, such as monoatomic motion on cluster facets, we interpolated reasonable barriers.

We permitted diffusion of Pd atoms that were directly in contact with the LiNbO_3 surface or on cluster facets. On the LiNbO_3 surface, we permitted the following diffusion processes: 1) nearest-neighbor monomer hopping, 2) agglomeration/deagglomeration (movement of Pd atom from layer 1 (2) onto layer 2 (1)), 3) dimer walking and sliding on c^+ , 4) trimer walking and sliding on c^+ , 5) trimer flipping on c^- , 6) tetramer rolling and 7) dissociation (some of these processes are pictured in Fig. 2 in the main text). On cluster facets, we permitted monomer hopping only. Though concerted movements of multiple atoms can occur on metal cluster facets, these generally affect cluster morphology, but not cluster size (number of atoms present). Since our primary interest is only in seeing differences in cluster size, this simplification of Pd behavior on cluster facets is acceptable.

It is well known that the activation barriers for monomeric diffusion on the (111) surfaces of FCC metals are quite low relative to the bulk metal-metal bond energy. Our nudged elastic band (NEB) calculations show that the activation barrier for monoatomic hopping from from FCC to HCP hollow sites on (111) surface of palladium is 0.11 eV, despite the fact that the Pd-Pd bulk bond energy is nearly six times larger (0.59 eV). This is explained by the fact that during monomer hopping between nearest-neighbor sites, new bonds start to form before others are completely broken. In our KMC simulations, we interpolated reasonable activation barriers for diffusion events on Pd cluster facets using insights from Trunshin and coworker's studies of nearest-neighbor

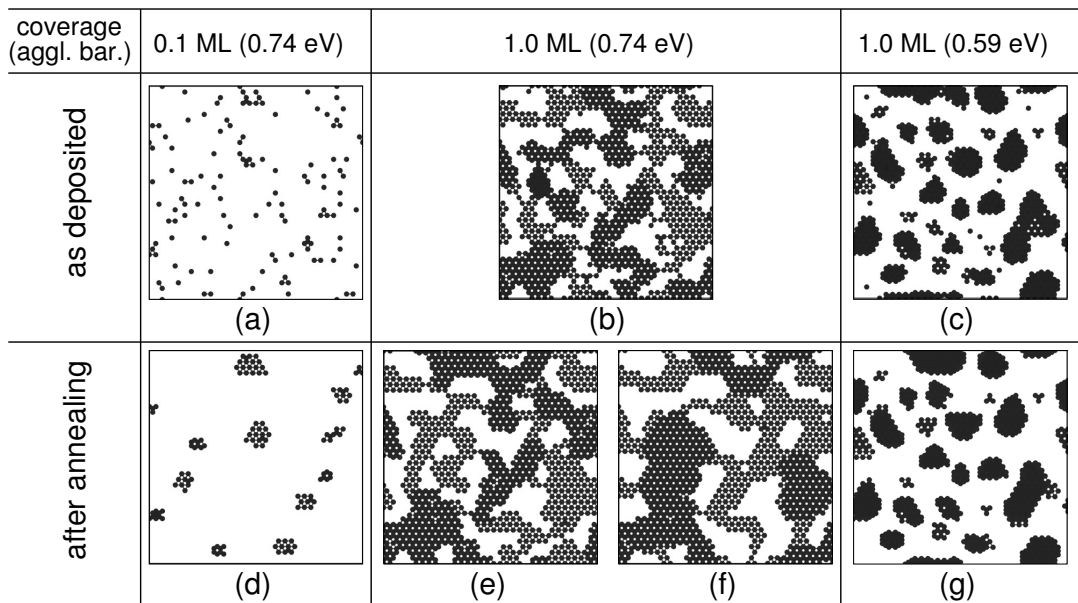


FIG. S3: Pd adsorption geometries predicted by kinetic Monte Carlo simulations on the c^- surface of LiNbO_3 immediately after deposition ends (a-c) and 2-15 minutes later (d-e). These simulations were conducted at different coverages (0.1 ML and 1.0 ML), different temperatures (300 and 400 K), and with the two different agglomeration barriers predicted by DFT (0.59 eV and 0.74 eV). All simulations were conducted at a deposition rate of 0.025 ML/s. Times waited after the completion of deposition were: (d) 15 minutes, (e) 10 minutes, (f) 2 minutes, and (g) 3 minutes. All simulations are conducted at 300 K, except for (f), which is at 400 K.

monoatomic hopping on copper surfaces and steps [8]. By compensating for the difference in cohesive energy between bulk Pd and Cu, we estimated that the activation barrier for nearest neighbor monomer hopping is 0.2 eV per Pd-Pd bond broken during transition state formation. We also showed that the qualitative results of some of our simulations were insensitive to the use of a 0.3 eV barrier for this process. In next nearest neighbor monomer hopping, which is analogous to the agglomeration processes pictured in Fig. 2 but generalized to movements between any two levels in the simulation lattice (starting with level 2), Pd-Pd bonds are broken completely during transition state formation. Thus, we estimated the activation barrier for this process based on the cost of Pd-Pd bond breaking. The cost of breaking a bond in a Pd_{20} cluster cut from bulk Pd is 0.52 eV. Similarly the cost of dimer dissociation is 0.55 eV. Thus, for next-nearest neighbor hopping on Pd cluster facets, we used a barrier of 0.5 eV per Pd-Pd bond broken.

AGGREGATION AND AGGLOMERATION ON c^- AFTER DEPOSITION

The relatively large diffusion barriers on the c^- surface (≈ 0.8 eV) were not sufficiently high to prevent agglomeration completely, especially when our simulations were extended until slightly after deposition was complete. We have conducted KMC simulations during deposition and

after annealing for 2-15 minutes for both low (0.1 ML) and high (1.0 ML) coverages and at different temperatures (300 or 400 K). We also conducted our simulations with agglomeration barriers (0.59 and 0.74 eV) for the two different possible cluster agglomeration processes predicted by DFT on the c^- surface (See Fig. 2(g,h) and Table I in the main text). These data are reported in Fig. S3.

At low coverage (0.1 ML), Pd atoms are highly dispersed at the end of deposition (Fig. S3(a)). However, within 15 minutes, all but two Pd clusters are immobile, suggesting that on a slightly longer time scale, all Pd atoms will join immobile clusters (Fig. S3(d)). However, these clusters are quite small compared to the single cluster that forms on the c^+ surface under the same conditions. Two factors contribute to the formation of smaller clusters on the c^- surface than on c^+ : lower maximum mobile cluster size, and the higher number density of clusters on the surface during deposition. On the c^+ surface, the mismatch between the distances between monomeric Pd binding sites and Pd-Pd equilibrium bond distances makes the activation barrier for motion of relatively large clusters rather low. For example, our predicted barrier for tetramer rolling was similar to that for monomer hopping, largely because this process requires movement of only one Pd atom out of a monomeric potential well. Other work suggests that this condition may be met by Pd clusters as large as 13 atoms [9], and thus, that clusters of this size may be mobile on the c^+ sur-

face. In contrast, the diffusion of clusters larger than a tetramer on the c^- surface requires breakage of at least two Pd-X bonds, making these diffusion events extremely unlikely on the time scale of deposition. A second factor contributing to the formation of large clusters on the c^+ surface is the fact that, because barriers for diffusion are so low, many diffusion events can occur during the average waiting time between addition of new atoms to the simulation cell on this surface. This means that only a few atoms at a time will be separate from the large immobile cluster, greatly reducing the probability that a second immobile cluster will form. The opposite is true on the c^- surface, where larger diffusion barriers mean that on average multiple Pd atoms are deposited inside the simulation cell between diffusion events of a single atom or cluster. As a result, many individual clusters are present in any given area of the simulation cell, promoting the formation of many small immobile clusters.

At high coverage (1.0 ML), Pd atoms continue to rearrange after deposition is complete until all atoms make at least three Pd-X bonds (Fig. S3(b,e)). Once this occurs, agglomeration can only occur on an extremely long time scale, because it requires breakage of multiple Pd-X bonds. Thus, the Pd coverage area of these clusters will remain relatively constant. This was true even when our surface was annealed at a higher temperature (400 K, Fig. S3(f)), consistent with the finding of Zhao and colleagues that the Pd geometry on the c^- surface is stable up to 425 K [10].

Even when we used the lower of our two agglomeration barriers predicted from DFT on the c^- surface (Fig. 2(g) in the main text), multiple distinct clusters formed at 1 ML coverage (Fig. S3(c,g)). At low coverage we observed results similar to those for the higher agglom-

eration barrier (Fig. S3(d)), but with taller individual clusters. Overall, our simulations with this lower agglomeration barrier on the c^- surface predicted Pd coverage areas that were substantially higher than those on the c^+ surface, but lower than the simulations on the c^- surface with the higher agglomeration barrier.

In sum, our DFT and KMC calculations predict that though Pd forms slightly three dimensional clusters on the c^- surface of LiNbO_3 , its overall adsorption pattern on this surface is much more dispersed than that on the c^+ surface.

* corresponding author: rappe@sas.upenn.edu

- [1] S. V. Levchenko and A. M. Rappe, Phys. Rev. Lett. **100**, 256101 (2008).
- [2] A. Saito, H. Matsumoto, S. Ohnisi, M. Akai-Kasaya, Y. Kuwahara, and M. Aono, Jap. J. Appl. Phys **43**, 2057 (2004).
- [3] H. J. Monkhorst and J. D. Pack, Phys. Rev. B **13**, 5188 (1976).
- [4] J. Ihm, A. Zunger, and M. L. Cohen, J. Phys. C **12**, 4409 (1979).
- [5] J. Nell and H. S. O'Neill, Geochimica et Cosmochimica Acta **60**, 2487 (1996).
- [6] C. Kittel, *Introduction to Solid State Physics* (John Wiley & Sons, Inc., 1996), seventh ed.
- [7] F. Furche, Phys. Rev. B **64**, 195120 (2001).
- [8] O. Trushin, A. Karim, A. Kara, and T. S. Rahman, Phys. Rev. B **72**, 115401 (2005).
- [9] W. Fan and X. Gong, Applied Surface Science **219**, 117 (2003).
- [10] M. S. H. Zhao, D. A. Bonnell, and J. M. Vohs, J. Vac. Sci. Technol. **27**, 1337 (2009).